

MTU: The Multifunction Tree Unit in zkSpeed for Accelerating HyperPlonk

Jianqiao Mo, Alhad Daftardar, Joey Ah-kiow, Kaiyue Guo,
Benedikt Bünz, Siddharth Garg, Brandon Reagen

New York University

{jm8782, ajd9396, ja4844, kg3209, bb, sg175, bjr5}@nyu.edu

Abstract

Zero-Knowledge Proofs (ZKPs) are critical for privacy preservation and verifiable computation. Many ZKPs rely on kernels such as the SumCheck protocol and Merkle Tree commitments, which enable their security properties. These kernels exhibit balanced binary tree computational patterns, which enable efficient hardware acceleration. Prior work has investigated accelerating these kernels as part of an overarching ZKP protocol; however, a focused study of how to best exploit the underlying tree pattern for hardware efficiency remains limited. We conduct a systematic evaluation of these tree-based workloads under different traversal strategies, analyzing performance on multi-threaded CPUs and a hardware accelerator, the Multifunction Tree Unit (MTU). We introduce a hardware-friendly Hybrid Traversal for binary tree that improves parallelism and scalability while significantly reducing memory traffic on hardware. Our results show that MTU achieves up to $1478\times$ speedup over CPU at DDR-level bandwidth and that our hybrid traversal outperforms as standalone approach by up to $3\times$. These findings offer practical guidance for designing efficient hardware accelerators for ZKP workloads with binary tree structures.

1. Introduction

Zero-Knowledge Proofs are cryptographic protocols that allow a prover to convince a verifier that a statement is true without revealing any additional information beyond the validity of the statement itself. ZKPs have emerged as a critical building block for privacy preservation and verifiable computation in both academia and industry. They have been widely adopted in privacy-focused blockchain platforms, such as Zcash [4] and Mina [8], and are increasingly explored in applications such as privacy-preserving machine learning [18]. As real-world deployments demand better performance and scalability, hardware-accelerated implementations have become increasingly important.

A key computational primitive in many modern ZKP protocols is SumCheck [36]. SumCheck plays a central role in a variety of ZKPs, including HyperPlonk [11], Spartan [33], Hyrax [37], and Libra [41]. In order to support SumCheck in the HyperPlonk protocol, several subroutines are required: Build MLE, MLE Evaluation, Multiplication

Tree, and Product MLE. These workloads are detailed in Section 3.1. These subroutines share a common computational pattern: they can all be expressed as balanced binary trees, where each internal node is a computation derived from its two children. In addition to these SumCheck-related operations, Merkle Tree commitments are another binary-tree-based primitive frequently used in ZKPs, blockchains, and secure storage systems, where hash-based commitments are built in hierarchical tree structures.

Balanced binary trees can be computed using either breadth-first (BFS) or depth-first (DFS) traversal strategies. While both are equivalent in algorithmic complexity, their behavior under hardware execution differs significantly due to resource constraints and memory hierarchy considerations. Prior theoretical research has primarily focused on aspects such as asymptotic complexity and software implementation [17]. However, designing hardware for these workloads requires careful consideration of several practical factors, including the ability to effectively exploit parallelism, memory traffic/bandwidth pressure, the complexity of control logic, the initiation interval in pipeline stages, and the ability to interface efficiently with upstream and downstream modules. These considerations are critical for achieving high performance but are relatively less studied in the binary tree workloads.

In this paper, we systematically evaluate binary tree workloads commonly used in ZKP, especially in SumCheck-related operations. We begin by analyzing the performance scalability of different traversal methods on the multi-threaded CPU. For hardware evaluation, we utilize the Multifunction Tree Unit (MTU) architecture [13] to assess the runtime and speedup of different traversal methods, as well as to explore the design space trade-offs between area and performance across a range of hardware configurations. Additionally, we analyze the hardware-friendly Hybrid traversal scheme that balances the benefits of both BFS and DFS, enabling efficient binary tree computation on MTU-based accelerators. Our key contributions are as follows:

- We analyze the hardware-friendly Hybrid traversal strategy that enables efficient, simple-control parallelism while significantly reducing memory traffic overhead.
- We evaluate four representative ZKP workloads – Build MLE, MLE Evaluation, Multiplication Tree,

and Merkle Tree Commitment – using different traversal methods.

- We perform a systematic hardware evaluation across memory bandwidth settings ranging from DDR to HBM, and complete a design space exploration of MTU. Our results show that MTU achieves a speedup of $1478\times$ over the CPU baseline with DDR-level bandwidth and that our Hybrid traversal outperforms BFS by nearly $3\times$.
- Our results offer insights into how traversal strategies affect runtime, bandwidth usage, scalability, and area efficiency, providing practical guidance for the hardware design of future ZKP accelerators.

These findings contribute to a deeper understanding of how to design and optimize hardware for cryptographic workloads with tree-based dataflows. The MTU accelerator demonstrates a compact hardware footprint. This efficiency enables MTU to be integrated into larger SoC designs or chiplet-based systems, sharing a common HBM PHY for memory access. It can be flexibly applied to future SumCheck accelerators or reused as a polynomial commitment engine across diverse ZKP stacks.

2. Background

2.1. ZKP and zkSNARKs

ZKPs are a privacy-preserving technology that allow a prover to convince a verifier that they know some information such that a statement is true. A similar application field is private ML [15, 16, 20, 27, 43]. The state-of-the-art ZKPs are defined as Zero-Knowledge Succinct Non-interactive ARgument of Knowledge (zkSNARKs), which offer small proofs and fast verifier time at high prover costs.

zkSNARKs are constructed from the combination of an interactive oracle proof (IOP) and a polynomial commitment scheme (PCS). The IOP provides a mechanism for the prover to encode a computation as an arithmetic circuit, and subsequently, as a set of polynomials whose evaluations can be efficiently checked through queries by the verifier. SumCheck [36] is a key kernel present in many recent IOPs due to its ability to scale efficiently with increasing problem complexity. Number-Theoretic Transform (NTT) [44] is an alternative to SumCheck used in some ZKP protocols. The PCS, in turn, binds the prover to these polynomials and enables the verifier to check the correctness without requiring access to the full polynomials. There are two common PCS kernels, Multi-Scalar Multiplication (MSM) and Merkle Tree. Together, IOPs and PCSs form the foundation of zkSNARK protocols such as HyperPlonk [11] and Orion [42]. We focus on workloads related to SumCheck and Merkle Tree, seen in HyperPlonk and Orion respectively, as they both contain binary tree computational patterns and can be accelerated using similar hardware.

2.2. SumCheck and MLEs

SumCheck [36] is an interactive protocol that allows a prover to convince a verifier that the sum of a multivariate

polynomial, $f(x_1, \dots, x_\mu)$, over the *boolean hypercube* is some claimed sum, S :

$$S = \sum_{x_1 \in \{0,1\}} \sum_{x_2 \in \{0,1\}} \cdots \sum_{x_\mu \in \{0,1\}} f(x_1, x_2, \dots, x_\mu) \quad (1)$$

The boolean hypercube is equivalent to a μ -bit space $\vec{x} \in \{0, 1\}^\mu$. At a high level, for a μ -variable polynomial f , there are μ rounds of the protocol; in round i , the prover makes a claim about the variable x_i . In zkSNARK protocols like HyperPlonk, a key constraint about f is that it is *multilinear*, meaning each variable’s maximum degree in f is one. A general representation of multilinear polynomials, for example, with $\mu = 3$,

$$\begin{aligned} f(x_1, x_2, x_3) = & f(0, 0, 0)(1 - x_1)(1 - x_2)(1 - x_3) + \\ & f(0, 0, 1)(1 - x_1)(1 - x_2)x_3 + \cdots \\ & + f(1, 1, 1)x_1x_2x_3 \end{aligned} \quad (2)$$

This representation defines polynomials using evaluations at specific input points (e.g., $f(0, 0, 1)$) rather than using coefficients. Additionally, the points can be stored as a *lookup table*, where each variable x_i can be interpreted as a bit. For example, $f(0, 0, 0)$ can be stored at index 0 in the table; $f(0, 1, 0)$ is stored at index 2.

Throughout SumCheck rounds, f will be evaluated at points where the variables x_i take values that are not limited to 0 or 1. Even though f is originally defined (and stored in hardware) over Boolean hypercube, the values of f at non-Boolean inputs will be extrapolated based on the values stored in the lookup table. These resulting values are called *extensions*, thus f is called a *multilinear extension* (MLE). The term *MLE table* denotes the corresponding lookup table structure mentioned above, where each entry can occupy 256 bits in ZKP applications.

In protocols like HyperPlonk, the polynomials upon which SumChecks are performed are often the result of tree-based compute patterns (e.g., Build MLE in Section 3.1.1). Therefore, a fast tree unit is essential to ensure these computational stages do not become a performance bottleneck in SumCheck-based protocols.

2.3. Merkle Tree Commitment

Merkle tree in ZKP allow a prover to commit to a large vector of data using a compact root hash. Each leaf node of the tree corresponds to a hashed element in the original vector, while each internal node is the cryptographic hash (e.g., SHA3 [6], Poseidon Hash [21]) of its two child nodes. This recursive construction culminates in a single root hash that serves as a commitment to the entire vector. Unlike MSM-based PCS constructions, Merkle trees do not require elliptic curve operations and thus typically offer faster prover runtime. However, this comes at the cost of increased proof sizes and slower verifier performance. Merkle-based PCS protocols, such as Orion [42], leverage this tradeoff by targeting environments where prover speed is critical and verifier costs are amortized or less constrained. Constructing a Merkle tree naturally maps to a binary tree reduction pattern. Similar to SumCheck, Merkle tree

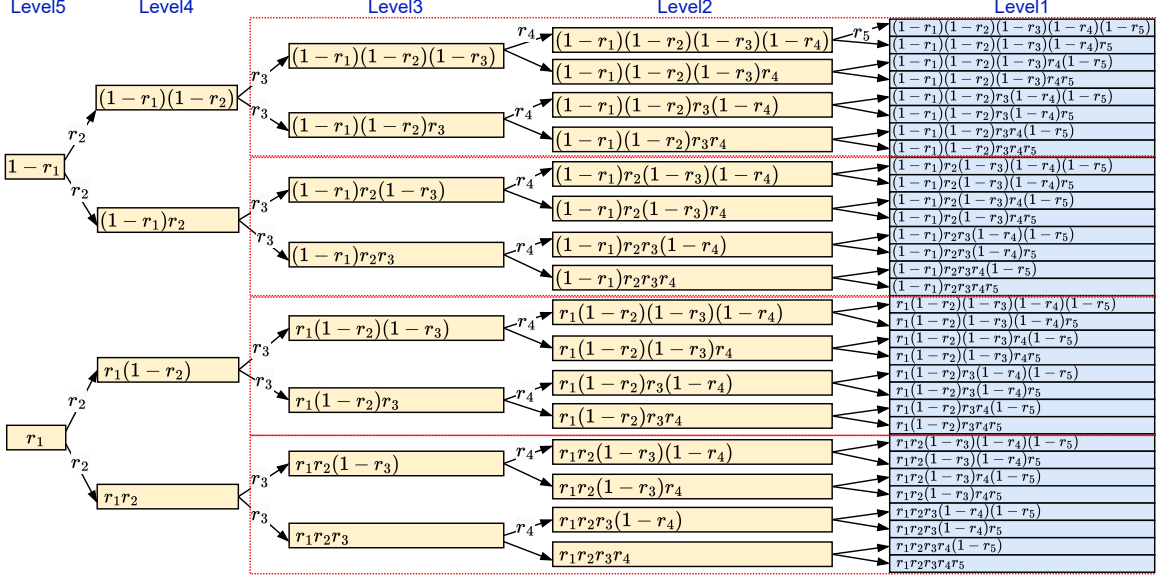


Figure 1: Dataflow for computing the Build MLE workload (output size 2^5) using a binary tree traversal. The result level (blue) is indexed as Level 1 and consists of 2^5 entries. An example partitioning into four subtrees is highlighted with red dash-boxes to illustrate parallel DFS processing.

construction benefits from an efficient tree unit, particularly when building large trees over vectors with lengths $\geq 2^{20}$.

3. Binary Tree Traversal

3.1. Binary Tree Workloads in ZKP

Balanced binary tree computations are prevalent in ZKP protocols, particularly in SumCheck-based constructions [11, 33]. These computation patterns appear repeatedly across ZKP applications and often form performance bottlenecks. Fortunately, their shared structure allows the design of a general hardware module that can accelerate them all with minimal specialization. zkSpeed introduces the MTU as a module capable to support multiple binary-tree-based computations. In this section, we highlight several common binary tree computations in ZKP that motivate the design of the MTU.

3.1.1. Build MLE. Build MLE is an important subroutine in accelerating SumCheck-related protocols. SumCheck allows the prover to prove the sum of a multivariate polynomial f over the Boolean HyperCube is zero, but in many ZKP protocols, the goal could be stronger: to prove that $f(\vec{x}) = 0$ for every Boolean HyperCube input, i.e., each lookup table entry evaluates to 0. However, running a SumCheck directly on $f(\vec{x})$ with a claimed sum $S = 0$ is not sufficient, because two terms might be nonzero yet cancel each other out, meaning the total sum is zero even if some of the individual evaluations are not zero.

To ensure correctness, a polynomial $\tilde{e}q(\vec{x}, \vec{r})$ is introduced [7, 11, 33, 34]:

$$\tilde{e}q(\vec{x}, \vec{r}) = \prod_{i=1}^{\mu} (r_i x_i + (1 - r_i)(1 - x_i)) \quad (3)$$

where $\vec{x} \in \{0, 1\}^{\mu}$, $\vec{r} \in \mathbb{F}^{\mu}$ are μ random values in \mathbb{F} finite field (challenges). By proving $\sum_{\vec{x} \in \{0, 1\}^{\mu}} f(\vec{x}) \cdot \tilde{e}q(\vec{x}, \vec{r}) = 0$ with SumCheck, it implies that $f(\vec{x}) = 0 \forall \vec{x} \in \{0, 1\}^{\mu}$. Its correctness is shown in [10, 33] and is known as a ZeroCheck in [11, 19]. We call the computation to construct $\tilde{e}q(\vec{x}, \vec{r})$ as *Build MLE*.

To perform ZeroCheck, the prover must evaluate $\tilde{e}q(\vec{x}, \vec{r})$ at all $\vec{x} \in \{0, 1\}^{\mu}$, which in fact are a list of products from $(1 - r_1)(1 - r_2) \cdots (1 - r_{\mu})$ to $r_1 r_2 \cdots r_{\mu}$. A naive approach requires $(\mu - 1)2^{\mu}$ modular multiplications to compute all such products individually. However, this cost can be reduced substantially by computing the values via a binary tree structure, as illustrated in Figure 1. The binary tree method reduces the number of modular multiplications to $2^{\mu+1} - 4$, providing significant computational savings. This optimization motivates the tree-based hardware design capable of efficiently supporting this pattern. In the tree-based computation, we can reduce one modular multiplication by using

$$(1 - r_1) \cdot (1 - r_2) = (1 - r_1) - (1 - r_1) \cdot r_2 \quad (4)$$

That is, $(1 - r_1)(1 - r_2)$ can be computed from $(1 - r_1)r_2$, instead of computing an extra modular multiplication with $(1 - r_2)$ and $(1 - r_1)$.

3.1.2. MLE Evaluation. MLE Evaluation is also an important step in SumCheck-related ZKP protocols. It is used to evaluate a multilinear polynomial on a given challenge point.

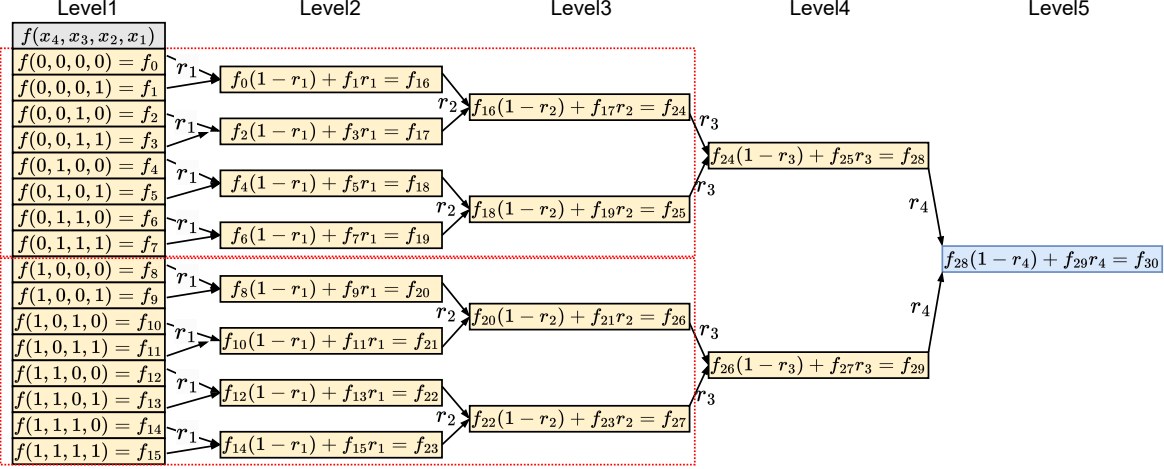


Figure 2: Dataflow for computing the MLE evaluation workload of input size 2^4 . The input level is indexed as Level 1, and the final output is highlighted in blue. An example partitioning into two subtrees is shown with red dash-boxes to illustrate parallel DFS processing.

Generally, there is a multilinear polynomial $f(\vec{x})$, and it is depicted by its values on the Boolean Hypercube (i.e., $f(\vec{x}) \forall \vec{x} \in \{0, 1\}^\mu$), in the form of a look-up table (see Section 2). The prover will be asked to evaluate f on a random challenge $\vec{r} \in \mathbb{F}^\mu$, i.e., to compute $f(r_1, r_2, \dots, r_\mu)$. Since f is a multilinear polynomial, as shown in Equation 2, the MLE Evaluation can be written as

$$f(r_1, \dots, r_\mu) = f(0, \dots, 0)(1 - r_1) \cdots (1 - r_\mu) + \dots + f(1, \dots, 1)x_1 \cdots x_\mu \quad (5)$$

A naive method is to modular-multiply every individual term and sum all at the end. Similar to Build MLE, we can substantially improve the computation by following the binary tree structure, while the tree is now inverted (reduction computation, as shown in Figure 2). With the binary tree structure, the number of modular multiplications can be optimized from $\mu \cdot 2^\mu$ to $2^\mu - 1$.

Note that in Figure 2 we also applied this trick to further reduce one modular multiplication.

$$f_0 \cdot (1 - r_1) + f_1 \cdot r_1 = f_0 + r_1 \cdot (f_1 - f_0) \quad (6)$$

Since modular addition is cheaper than modular multiplication, we can replace the original form on the left of the equation with only one mod-mul on the right.

3.1.3. Merkle Tree. The Merkle tree is a widely used cryptographic commitment scheme in which the root of a binary tree serves as the commitment to a set of leaf values. Individual leaves can later be revealed and efficiently verified as part of the committed structure using authentication paths. In the context of ZKP protocols, Merkle trees are often employed as hash-based polynomial commitment schemes.

Unlike MLE Evaluation in Equation 5, the Merkle Tree naturally has a binary tree structure. The Merkle tree commitment workload follows a similar computation

pattern as illustrated in Figure 2. The primary difference lies in the operation at each node: Level 1 consists of the hash values of the original input data, and each subsequent level is computed by hashing pairs of nodes from the previous level. Instead of modular arithmetic, each tree node performs a cryptographic hash of its two child nodes, forming a hierarchical hash structure that culminates in a single root commitment. This structural similarity enables reuse of binary-tree acceleration strategies for Merkle tree construction and verification within zero-knowledge systems.

3.1.4. Multiplication Tree and Product MLE. Binary tree-style product computations are not limited to Sum-Check protocols; many cryptographic algorithms require computing products of the form $\prod_{i=0}^{2^\mu-1} f_i$. In cryptographic contexts, these products typically involve modular multiplication, which is significantly more expensive than standard integer multiplication. A simple way is to accumulate the product one by one, which will incur a high latency because of the data dependency. Therefore, it is crucial to optimize such computations using binary tree structures to reduce computational cost.

One notable example is the *Product MLE* computation in HyperPlonk, which resembles a standard multiplication tree. However, unlike a typical tree that only outputs the final product at the root, the Product MLE computation requires the outputs from *all* intermediate levels of the tree. These intermediate values are essential for downstream steps in the protocol. The multiplication tree and Product MLE workloads follow a similar structural pattern to that shown in Figure 2, with the primary difference in the node operation. Instead of modular addition and multiplication, each simply computes a modular multiplication of two nodes from the previous level. The Product MLE workload requires outputting the intermediate results (levels starting from Level 2), which increases bandwidth demands.

Table 1: DIFFERENT BINARY TREE TRAVERSAL METHODS.

Traversal	BFS	DFS	MTU Hybrid
Time Complexity	$O(n)$	$O(n)$	$O(n)$
Parallel Control	Easy	Hard	Medium
Initiation Interval	=1	>1	=1
Input indices	Continuous	Discont.	Continuous
Memory Cost	High	Low	Low
Bandwidth Cost	Linear to #PEs	Fixed	Fixed

SumCheck. At each round i of the SumCheck protocol, one might observe that the summation $\sum_{x=0}^{2^i-1} f(x)$ follows a tree-based reduction pattern. However, unlike modular multiplication, modular addition is relatively inexpensive and incurs minimal latency (e.g., in zkSpeed [13], mod-add has only one stage pipeline). As a result, the accumulation dependency does not significantly impact the throughput or total latency. A simple accumulator is therefore sufficient to compute the sum efficiently, without the need for a full binary reduction tree. The modular multiplication has a ten-stage pipeline, thus the accumulator method would significantly influence the latency.

3.2. General Binary Tree Traversals

Binary tree computations can be traversed in various ways, with the two most common strategies being breadth-first search (BFS, or level-order traversal) and depth-first search (DFS, including inorder, preorder and postorder traversal). In DFS, computation progresses by recursively visiting one branch of the tree down to its leaves before backtracking. In contrast, BFS processes the tree level by level, evaluating all nodes at a given depth before moving to the next.

BFS. Each traversal strategy offers trade-offs. BFS is straightforward to implement and control, making it a natural choice in software for binary tree workloads mentioned above. Its dataflow typically involves reading all nodes at a given level from memory, performing computations in parallel, and then writing results back to memory. In the example of Figure 2, BFS computation follows Level 2, 3 and so on. This regular, level-by-level structure is amenable to parallelism. However, BFS has significant hardware design challenges. If implemented entirely on-chip, it requires storing all intermediate levels of the tree, which can incur prohibitive memory costs. For example, processing Build MLE of 2^{23} workload size would require 128 MB of on-chip SRAM, and it grows linearly with the size. This is inefficient for typical ASIC designs. Alternatively, if intermediate levels are stored off-chip, the design becomes bandwidth-limited, and the achievable parallelism is constrained by memory access throughput. These limitations motivate the need for more memory-efficient traversal strategies that balance parallelism with resource constraints. Hardware accelerators like Nocap [31] applied BFS for its Merkle tree computation.

DFS. DFS offers substantial memory and bandwidth savings compared to BFS through on-chip data reuse. Since DFS computes each branch to completion before moving on, intermediate results are consumed immediately and do

not need to be stored for long durations. For example in Figure 2, it follows the order f_0, f_1 to f_{16} , and then f_2, f_3, f_{17}, f_{24} , and so on. Due to the data dependency, DFS is naturally less compatible with parallel hardware execution. A naive approach (i.e., allocating multiple PEs and feeding them in DFS order) will result in complex scheduling and high latency due to deep recursive computation. Initial inputs will be interrupted since the PE prioritizes the process of the deeper level. The arrival rate of the initial inputs becomes irregular, leading to an initiation interval (II) greater than one, where not all PEs can accept new initial input data every cycle.

One way to simplify DFS-based scheduling is to divide the tree into multiple subtrees and assign each subtree to a dedicated PE. In Figure 2, we divide the workload into two subtrees as shown in the red dash-boxes, which enables two parallel PEs to compute each subtree, and their results will be merged at the end. Figure 1 is similar, while the Level 4 will be first prepared and then distributed to parallel PEs to compute each subtree. This can improve concurrency, but since the tree is divided into several subtrees, the initial input or output indices are no longer sequential. If an upstream module (e.g., another accelerator block) is producing tree inputs in strict index order, such DFS traversal cannot be directly pipelined with it, limiting throughput. These challenges highlight the need for traversal strategies that preserve DFS’s reuse efficiency while improving input regularity and pipelining compatibility. Hardware accelerators like UniZK [38] applies similar philosophy of dividing tree, but within each subtree it still performs BFS individually.

These traversal strategies are summarized in Table 1. Importantly, regardless of the traversal method, the asymptotic time complexity remains the same $O(n)$ since each approach must visit all n nodes in the tree once [17]. Ideally, parallelism may improve this latency to $O(n/p)$ for p parallel PEs. The key differences lie in space complexity and their suitability for parallel execution. BFS enables straightforward parallelism across tree levels but incurs a space complexity of $O(n)$ due to the need to store a level of intermediate data. In contrast, DFS has lower memory requirements because intermediate results can be reused and discarded quickly, but it presents greater challenges in coordinating parallel execution and achieving efficient pipelining.

4. Hardware-Friendly Hybrid Traversal

To balance the trade-offs between space complexity and parallelism, MTU introduces a hybrid traversal strategy tailored for hardware efficiency. This method combines the low-memory advantages of DFS with the parallelism-friendly nature of BFS to reduce overall traversal time.

The starting point of our design is rate-matching the upstream. For an inverted binary tree as in Figure 2, if eight nodes of Level 1 arrive per cycle, four PEs will be allocated to process them in parallel, and two PEs are used for the second level, and one PE for the third level. As

Table 2: SCHEDULING OF MTU DFS ACCUMULATOR WHEN PROCESSING AN INVERTED BINARY TREE. L_4 MEANS THE INDEX-0 NODE OF LEVEL 4. THE PE TAKES TWO INPUTS FROM PREVIOUS LEVEL, AND PRODUCE ONE OUTPUT AS THE NEXT LEVEL.

Cycle	0	1	2	3	4	5	6	7	8	9	10	11	12	13	14	15	16	17	18	19	20	21	22	23	24	25	26	27	...
Input A	L_4	-	L_2	-	L_4	L_5	L_6	-	L_8	L_5	L_{10}	L_6	L_{12}	L_5	L_{14}	-	L_{16}	L_6	L_{18}	L_6	L_{20}	L_8	L_{22}	L_7	L_{24}	L_{10}	L_{26}	...	
Input B	L_1	-	L_3	-	L_5	L_7	-	L_9	L_5	L_{11}	L_6	L_{13}	L_5	L_{15}	-	L_{17}	L_7	L_{19}	L_6	L_{21}	L_9	L_{23}	L_7	L_{25}	L_{11}	L_{27}	...		
Output	-	L_5	-	L_1	-	L_5	L_6	L_3	-	L_4	L_6	L_5	L_7	L_6	L_7	-	L_8	L_6	L_9	L_9	L_7	L_{10}	L_6	L_{11}	L_8	L_{12}	L_6	...	

Table 3: SCHEDULING OF MTU DFS ACCUMULATOR WHEN PROCESSING A FORWARD BINARY TREE (BUILD MLE). L_7 MEANS THE INDEX-0 NODE OF LEVEL 7. THE PE TAKES AN INPUT FROM PREVIOUS LEVEL, AND PRODUCE TWO OUTPUTS AS THE NEXT LEVEL.

Cycle	0	1	2	3	4	5	6	7	8	9	10	11	12	13	14	15	16	17	18	19	20	21	22	23	24	25	26	27	...
Input	L_8	-	-	L_7	-	L_6	-	L_5	L_6	L_5	L_7	L_5	L_6	L_5	L_8	L_4	L_5	L_6	L_5	L_7	L_6	L_4	L_5	L_7	-	L_8	L_6	L_9	...
Output A	-	L_7	-	-	L_6	-	L_5	-	L_4	L_5	L_4	L_6	L_4	L_5	L_6	L_4	L_5	L_6	L_{10}	L_6	L_{12}	L_8	L_{14}	-	L_{16}	L_{10}	L_{12}	...	
Output B	-	L_7	-	-	L_6	-	L_5	-	L_4	L_5	L_4	L_6	L_4	L_5	L_6	L_4	L_5	L_6	L_{11}	L_6	L_{13}	L_9	L_{15}	-	L_{17}	L_{11}	L_{13}	...	

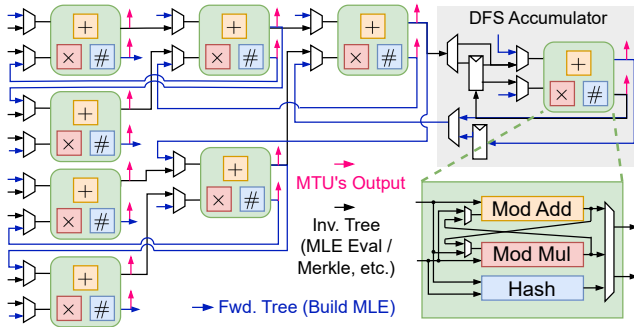


Figure 3: An example architecture of the MTU with 8 PEs for Hybrid Traversal. Each PE supports both modular arithmetic and hashing. Their connection enables both forward and inverted binary trees computation. All PEs are interconnected to support pipelined dataflow and can directly output results of the accelerator.

shown in Figure 3, these seven PEs are connected to form a pipeline, enabling the first to third levels to be grouped and computed in a BFS fashion. That is, nodes in Level 1 to 3 are grouped (as the red dash-boxes in Figure 2), and processed by the seven PEs pipeline. Starting from the fourth level, the generation rate naturally becomes one per cycle, which aligns with the capacity of a single PE, making DFS a suitable choice for deeper levels. Thus, the traversal is divided: the input levels are handled using BFS to match the Level 1 input rate and ensure continuous input indexing. The intermediate data are reused in the pipeline. On the other hand, the deeper levels (starting at Level 4) adopt DFS which has low space complexity. This hybrid scheme maintains parallelism with low space complexity, avoids off-chip bandwidth bottlenecks through on-chip reuse, and simplifies scheduling and control logic. It eliminates the need to store entire intermediate levels, making it practical for large problem sizes. Furthermore, the design is scalable, as the number of PEs can be adjusted to match the input rate, forming a full pipeline with other accelerator units.

4.1. MTU Architecture

In this section, we present the architecture of MTU. Figure 3 illustrates an example configuration. The MTU is composed of several PEs that are connected to support both

standard (forward) and inverted binary tree traversals. In Figure 3, the inverted tree mode (workloads like Merkle tree commitments, multiplication tree) MTU can accept eight inputs per cycle. That is, the PEs will take eight elements of Level 1 (e.g., f_0 to f_7 in Figure 2) into the pipeline each cycle, and produce a Level 4 element (e.g., f_{28}) into the last PE to work in DFS. The architecture can be extended on demand. Putting more PEs in the front allows the MTU to process more inputs per cycle. Each PE is equipped with a SHA3 engine to accelerate hash-based operations required in Merkle Tree, along with modular addition and multiplication units to support arithmetic workloads (e.g., MLE Evaluation and Multiplication Tree).

Scheduling. We show the scheduling of MTU’s DFS Accumulator PE in Table 2, assuming an MTU configuration as Figure 3 and the PE latency is one cycle. For a large inverted binary tree (e.g., 2^{20} nodes in Level 1), since Level 4 elements come at one per cycle, the generation of Level 5 happens every two cycles, as well as the Level 6 happens every four cycles and so on. The temporary result (e.g., L_5) will be buffered in a small SRAM and consumed once the input pair is ready to launch. This give us a chance to interleave to schedule levels. The scheduling depends on the “generation rate” of each level. It can be efficiently handle by a simple controller, which prioritizes the computation of a deeper level. If the inputs of a deeper level are ready, it will be triggered to compute. Initially, there are gaps in the scheduling, as it must wait two cycles for each input pair. However, once multiple levels are processed, the gaps will be filled. Each PE is also connected to the output ports (red wires in Figure 3) to support Product MLE computation, which requires all elements of every level.

On the other hand, in the forward binary tree (for operations like Build MLE), the MTU can generate up to eight outputs per cycle. PEs are connected in blue wires in Figure 3. Different from the inverted binary tree, here the four PEs on the left are generating the output level (i.e., Level 1). Nodes in Level 3 to 1 are grouped (as the red dash-boxes in Figure 1), and processed by the seven PEs pipeline. Following the similar DFS scheme, the last PE accumulator is used to generate Level 4 and above. Its scheduling is illustrated in Table 3. Nodes of Level 4 are produced at an average rate of one per cycle, which enables the computation of Level 3 to be launched every cycle. As

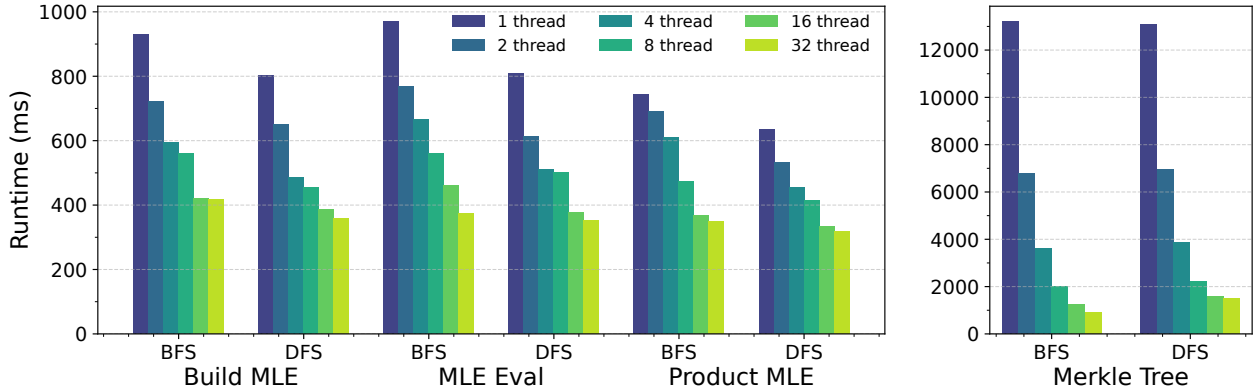


Figure 4: CPU performance across different workloads using BFS and DFS traversal schemes. Each workload is evaluated at size 2^{20} .

a result, eight elements of Level 1 can be output at the end in a continuous stream.

The MTU Hybrid traversal, working with the DFS Accumulator PE, enables recursive computation of deeper levels with minimal memory overhead. Its scheduling follows a fixed pattern, simplifying control logic. The key design insight is to match the generation rates between adjacent levels: nodes in Levels 1 to 3 are processed in groups by the pipeline formed from the seven PEs, while the DFS Accumulator PE works by aligning its input or output rates with the group of seven PEs.

5. Methodology

In this section, we detail our experimental setup for evaluating the MTU architecture.

Simulation and Workloads. We evaluate MTU using the representative workloads described in Section 3.1. Software performance is measured on Intel Xeon Gold 5218 CPU [24] with Thermal Design Power (TDP) 125 W, and DDR4 memory. The baseline software implementation is built on top of the HyperPlonk and the arkworks Rust library [3, 45]. Software multi-threaded tests are handled by Rayon. To explore scalability, we evaluate the CPU baseline with thread counts ranging from 1 to 32, and compare it against MTU configurations using 2 to 32 PEs. Since MTU uses hybrid binary tree traversal with a DFS Accumulator, we start from a configuration with 2 PEs. We do not evaluate Hybrid traversal on the CPU, as it lacks the tight pipeline structure of hardware PEs, making it infeasible for the precise scheduling required for the DFS Accumulator stage in Hybrid traversal. To reflect realistic system memory conditions, we simulate MTU performance under various bandwidth constraints, ranging from 64 GB/s (comparable to CPU systems with DDR4 [9, 29] and DDR5 [32]) to 1024 GB/s (HBM-class memory [1, 23, 25, 28]). This allows us to evaluate MTU’s performance potential across both commodity and high-end memory environments.

Hardware Implementation. We design a cycle-accurate simulator to model MTU’s hybrid traversal, as discussed

in Section 4, together with a scheduler to control the task for the DFS accumulator in MTU. Our simulation uses 255-bit datatypes, consistent with the finite field setting in HyperPlonk. We use Catapult HLS 2023 to generate fully-pipelined Montgomery multipliers supporting arbitrary prime moduli (following prior work [13, 14]). For hash computations in Merkle Tree, we instantiate the SHA3 block from OpenCores [30]. On-chip memory is modeled using SRAM estimates generated by Synopsys 22 nm Memory Compiler. Area and power figures are scaled to 7 nm using technology scaling factors: $3.6\times$ for area, $3.3\times$ for power, and $1.7\times$ for delay [12, 14, 39, 40]. The MTU is assumed to operate at a clock frequency of 1 GHz.

6. Evaluation

In this section we evaluate each workload with different traversal methods on CPU and MTU. We demonstrate the performance scaling on CPU threads, and the hardware performance scaling with constraint bandwidth.

6.1. Traversal Analyses on CPU

We first evaluate various binary tree traversal schemes on a CPU. Figure 4 presents the runtime performance for four representative workloads: constructing the Build MLE (resulting in an MLE table of size 2^{20} entries), evaluating the MLE, computing the Product MLE, and performing Merkle Tree commitment, each over an input table of size 2^{20} . By varying the number of CPU threads, we compare the traversal and analyze how traversal methods benefit from parallelism.

Among the workloads, the Merkle Tree shows clear performance scaling with increased thread count. In contrast, workloads involving modular arithmetic – such as Build MLE, MLE evaluation, and Product MLE – do not scale linearly with threads. This difference stems from the nature of the underlying computation: the SHA3 hash used in the Merkle Tree is well-optimized on modern CPUs via intrinsic SHA Extensions [22] and benefits significantly from thread-level parallelism, whereas modular arithmetic

operations are computationally intensive with more computation dependency.

The performance difference between BFS and DFS traversal is not pronounced, especially for large, compute-heavy workloads like Merkle Tree commitment, where most of the execution time is dominated by computation. The overhead introduced by traversal patterns becomes relatively minor in the overall execution time. Nevertheless, DFS shows a modest runtime advantage (typically under 200 ms). This is attributed to two factors. First, in BFS, each tree level is processed using Rayon’s parallel iterators. While this simplifies parallelization, it introduces scheduling overhead: threads are spawned at each level of the tree, causing latency from synchronization and load balancing. In contrast, DFS implementation statically partitions the binary tree into independent subtrees, each assigned to a thread before the recursion. This allows threads to proceed without interruption, thus improving efficiency. Second, DFS achieves better cache locality compared to BFS. As discussed before, BFS traversal has fewer local reuse and accesses cross-level caches to store a large amount of data. In contrast, DFS naturally promotes sequential and localized memory access due to its recursive structure, allowing intermediate data to be consumed quickly. This increases the likelihood of cache hits and leads to more efficient execution for large workloads. While these advantages do not drastically change the overall asymptotic runtime, they could contribute to a consistent latency difference in practice.

Overall, the performance difference between BFS and DFS is minor for these workloads, as the computations are already dominated by intensive modular arithmetic or cryptographic hashing. In such compute-bound scenarios and large-size workloads, the traversal strategy contributes only marginally to total runtime. This observation suggests that traversal choices may matter more in memory- or bandwidth-bound contexts, especially in hardware accelerators where compute-latency is greatly improved.

6.2. MTU Parallel Execution and Speedup

We now evaluate the performance of the MTU hardware design across different numbers of processing elements (PEs), traversal strategies, and memory bandwidth constraints, ranging from DDR-level (64 GB/s) to HBM-scale (1024 GB/s). As in Section 6.1, we consider four representative ZKP workloads: Build MLE, MLE evaluation, Product MLE, and Merkle Tree commitment, each with a workload size of 2^{20} . Figure 5 shows the runtime results under these varying configurations. For the BFS traversal, each PE operates independently on nodes of the same tree level. In contrast, in the DFS traversal, each PE processes a disjoint subtree (as illustrated in Figure 1 and 2), and a final PE merges the results. The MTU’s Hybrid traversal, combines BFS and DFS to balance memory reuse and parallelism. We start from two PEs as it needs at least two PEs to build Hybrid traversal in MTU.

Traversal Comparison. We first analyze the difference between traversal methods. Under constrained bandwidth

(e.g., 64 GB/s) and low parallelism (2 PEs), both DFS and Hybrid traversals significantly outperform BFS. This is because BFS reads and writes each tree level to off-chip memory, making it heavily bandwidth-bound even with a single PE. In contrast, DFS and Hybrid traversals retain intermediate values on-chip and only access off-chip memory for the initial input (or final output in the case of Build MLE), avoiding bandwidth-induced stalls. An exception is the Product MLE workload, where it takes every tree level (including the intermediate levels) as output results. Therefore, even in DFS and Hybrid modes, performance becomes bandwidth-limited due to the increased off-chip traffic for outputs storing. On the other hand, in a high-bandwidth regime (1024 GB/s) with 2 PEs, traversal choice makes little difference, as all variants become compute-bound by the PE. For workloads except Product MLE, the DFS and Hybrid traversals achieve nearly $3\times$ speedup over BFS, with sufficient bandwidth and compute resources.

Scalability with PE Parallelism. The difference between traversals can be further evaluated by scaling the number of PEs under both bandwidth constraints. At 64 GB/s, increasing the PE count yields little benefit across all traversal methods due to memory bandwidth saturation. With 1024 GB/s, the performance scales with PE count; however, BFS saturates quickly – plateauing after 16 PEs – because of its bandwidth-heavy nature. Product MLE workload exhibits similar limitations after 16 PEs, even under DFS or Hybrid traversal, since its per-level output demands high sustained bandwidth. For the other workloads, DFS and Hybrid traversals scale more effectively beyond 16 PEs, demonstrating better bandwidth efficiency.

Although DFS and Hybrid deliver comparable performance, it is important to note a key limitation of DFS: it assumes the input is divided into disjoint subtrees. This assumption makes DFS unsuitable when the upstream component delivers inputs in a contiguous, streaming fashion. In contrast, Hybrid traversal supports both parallelism and continuous input indexing, making it more practical in pipeline-integrated systems.

Our evaluation also reveals the significant impact of memory bandwidth on performance scalability. With 32 PEs, the system becomes bandwidth-bound – performance is limited unless sufficient memory bandwidth is provisioned. As shown in Figure 5, increasing the bandwidth from 64 GB/s to 1024 GB/s enables near-linear scaling, as the additional bandwidth alleviates the data movement bottleneck and allows the hardware to maintain high utilization across all PEs.

Speedup over CPU. We compare the performance of MTU against the CPU baseline under matched PE/thread configurations. For the CPU, we select the best-performing traversal method as the baseline. On the hardware side, we evaluate MTU at two bandwidth levels: 64 GB/s, which is comparable to typical DDR4 memory bandwidth on CPUs, and 1024 GB/s, representing HBM-class bandwidth to illustrate the performance ceiling of MTU. Speedup results are shown in Figure 6.

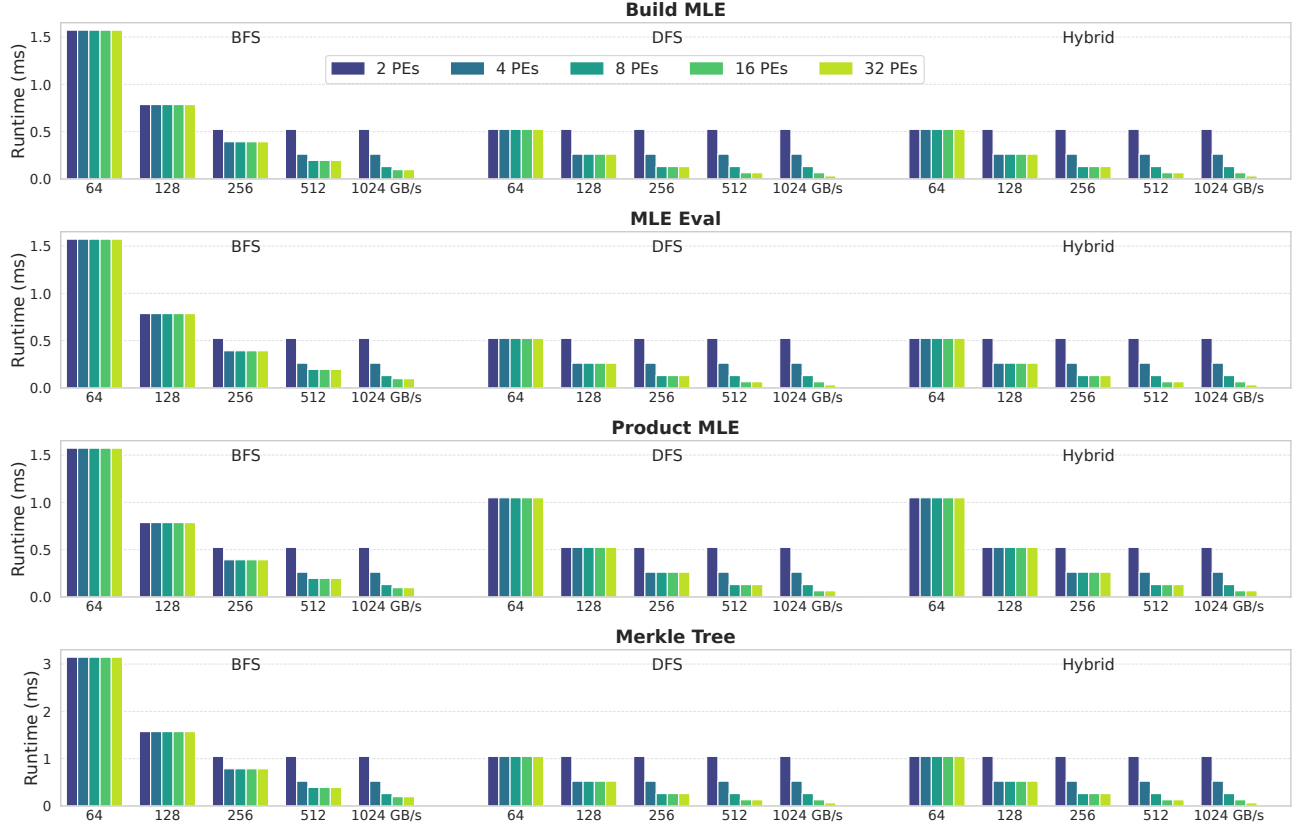


Figure 5: MTU runtime results across different workloads (each size 2^{20}), grouped by different traversals. Each group shows hardware runtime under varying hardware bandwidths and PE counts. We start from 2 PEs to perform Hybrid traversal.

The observed speedup trends mirror the hardware runtime patterns as discussed earlier. Notably, under the 64 GB/s bandwidth constraint, MTU’s speedup diminishes as the number of PEs increases. This is because the hardware falls bandwidth-bound, limiting performance gains despite additional PEs. Meanwhile, CPU performance continues to scale with increasing threads, as the workload remains compute-bound (as shown in Figure 4). Consequently, the relative hardware speedup decreases when CPU runtime improves with additional threads.

Overall, under CPU-level bandwidth conditions (64 GB/s), MTU with Hybrid traversal achieves an average speedup of $1478\times$ over the CPU baseline. When provisioned with high bandwidth (1024 GB/s), MTU can scale significantly better, reaching up to $9440\times$ average speedup against CPU due to its efficient high parallelism and sufficient memory bandwidth.

6.3. Area, Power and Pareto Space Analysis

Figure 7 illustrates the runtime versus area design space of MTU under various bandwidth configurations and PE counts, using the Hybrid traversal scheme. We sweep a range of bandwidths (from 64 GB/s to 1024 GB/s) and evaluate the design points using the Merkle Tree commit

workload with a problem size of 2^{20} . Other workloads have similar Pareto trends as well.

The figure demonstrates a clear trend: increasing available bandwidth reduces runtime and shifts the Pareto front to the left. For large-area configurations (i.e., higher PE counts), additional bandwidth yields greater performance gains. However, for designs below 3 mm^2 , the Pareto fronts across several bandwidth levels start to overlap, indicating that high bandwidth is not always necessary. For instance, a design slightly larger than 1 mm^2 achieves comparable performance under 256 GB/s and 1024 GB/s, suggesting that modest bandwidth suffices for smaller configurations.

Prospect of MTU. Table 4 summarizes the area and thermal design power of a representative MTU configuration with 32 PEs. MTU exhibits a compact footprint, and its area can be further reduced under limited bandwidth settings by scaling down the number of PEs. This enables MTU to be embedded within a larger SoC or included as part of a chiplet-based system while sharing a common HBM PHY interface for off-chip memory access. For example, MTU is integrated into the zkSpeed accelerator [13] to support ZKP proof generation. Beyond this case, MTU can be deployed to support potential SumCheck accelerators for MLE-related computation, or repurposed as a polynomial commitment engine within broader ZKP hardware stacks.

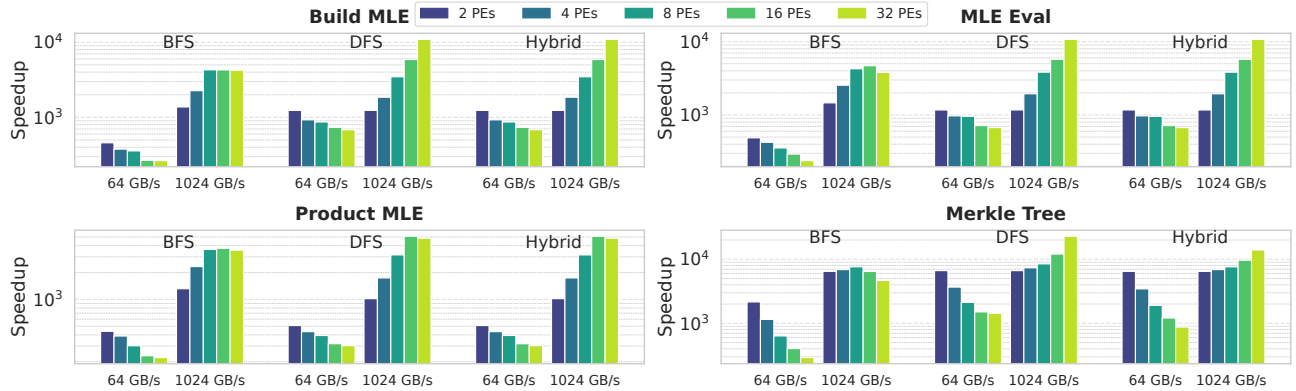


Figure 6: Hardware speedup over CPU baseline on workloads of size 2^{20} each, grouped by different traversals. Each group shows hardware performance under two bandwidth settings: DDR-level (low) and HBM-level (high). We start from 2 PEs to perform Hybrid traversal.

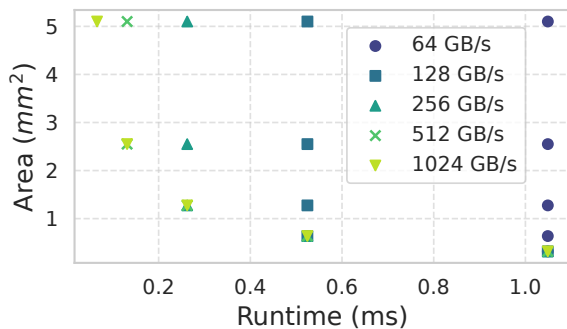


Figure 7: Runtime-area design space of MTU using Hybrid traversal on the Merkle Tree Commit workload. Each point represents a design configuration with a number of PEs and bandwidth. The Pareto frontier illustrates the trade-off between runtime and area across different bandwidth settings.

Table 4: AREA AND THERMAL DESIGN POWER (TDP) BREAKDOWN OF MTU HARDWARE CONFIGURED WITH 32 PEs.

Component	Area (mm ²)	TDP (W)
Modulus Ops	4.427	6.886
SHA3	0.192	0.320
Misc	0.416	0.649
Memory	0.067	0.003
Total MTU	5.101	7.857
HBM2 PHY	14.90	0.225

Its versatility and compactness make MTU a promising building block for modular ZKP accelerator architectures across a range of proof systems and deployment platforms.

7. Related work

Several prior works have explored hardware acceleration for ZKP protocols across various platforms and protocol families. **SZKP** [14] accelerates the Groth16 protocol by

optimizing MSM using Pippenger’s algorithm and dedicated scheduling strategies. MSM over elliptic curves serves as a PCS alternative to Merkle Tree-based commitments, offering smaller proof sizes but at higher computational cost. **NoCap** [31] proposes a vector-based processor targeting Spartan+Orion ZKP protocols. These protocols rely on SumCheck and Merkle Tree as core building blocks. While NoCap supports SumCheck, it does not provide specialization for SumCheck subroutines such as Build MLE or MLE evaluation. Merkle Tree computation is mapped to the vector engine directly using level-order BFS traversal. However, NoCap uses 64-bit datatypes while our implementation targets 255-bit. **zkSpeed** [13] is an ASIC accelerator that targets HyperPlonk. It performs end-to-end acceleration of proof generation, with dedicated modules for MSM, SumCheck and its associated subroutines. **UniZK** [38] presents a systolic-array-based architecture that accelerates NTT and Merkle Tree. It optimized the Merkle Tree by partitioning a tree into subtrees, and executing each subtree on-chip with BFS. UniZK uses Poseidon hash, whereas both NoCap and MTU use SHA3.

Several prior works have explored traversal optimizations to address application-specific constraints. Optimizations in [5, 26] aim to improve efficiency when the total workload size is unknown and reduce redundant hash computations by speculating on future authentication paths. Other hardware-focused work [35] improves Merkle Tree updates by reducing unnecessary memory traffic through cache-aware designs. For non-cryptographic workloads, for example, [2] proposes switching between BFS and DFS during Random Forest training depending on the active sample size. While these optimizations are effective for their target applications, a unified hardware evaluation of traversal strategies is not provided for the diverse tree-based workloads in modern ZKP protocols.

8. Conclusion

We presents a systematic evaluation of binary tree-based workloads in ZKP, focusing on traversal strategies and hard-

ware design trade-offs on MTU. Our results demonstrate that traversal strategies significantly impact performance, and that the proposed Hybrid Traversal achieves substantial improvements in both runtime and memory efficiency. Using the MTU architecture, we show up to $1478\times$ speedup over CPU baselines under DDR-level bandwidth. These findings offer practical insights for future ZKP accelerator designs and highlight the potential of tree units like MTU in modular ZKP hardware stacks. Its generality, efficiency, and portability makes MTU a promising building block for modular ZKP hardware platforms.

References

- [1] “High bandwidth memory dram (hbm3),” JEDEC, Technical Report JESD238A, 2023, <https://www.jedec.org/standards-documents/docs/jesd238a>.
- [2] A. S. Anghel, N. Ioannou, T. Parnell, N. Papandreou, C. Dünner, and H. Pozidis, “Breadth-first, depth-next training of random forests,” in *Annual Conference on Neural Information Processing Systems*, 2019.
- [3] arkworks contributors, “arkworks zkspark ecosystem,” 2022. [Online]. Available: <https://arkworks.rs>
- [4] E. Ben-Sasson, A. Chiesa, C. Garman, M. Green, I. Miers, E. Tromer, and M. Virza, “Zerocash: Decentralized anonymous payments from bitcoin,” in *2014 IEEE Symposium on Security and Privacy, SP 2014, Berkeley, CA, USA, May 18-21, 2014*. IEEE Computer Society, 2014, pp. 459–474. [Online]. Available: <https://doi.org/10.1109/SP.2014.36>
- [5] P. Berman, M. Karpinski, and Y. Nekrich, “Optimal trade-off for merkle tree traversal,” *Theoretical Computer Science*, vol. 372, no. 1, pp. 26–36, 2007.
- [6] G. Bertoni, J. Daemen, M. Peeters, and G. Van Assche, “Keccak specifications,” *Submission to nist (round 2)*, vol. 3, no. 30, pp. 320–337, 2009.
- [7] A. J. Blumberg, J. Thaler, V. Vu, and M. Walfish, “Verifiable computation using multiple provers,” *Cryptology ePrint Archive*, 2014.
- [8] J. Bonneau, I. Meckler, V. Rao, and E. Shapiro, “Mina: Decentralized cryptocurrency at scale,” *New York Univ. O (1) Labs, New York, NY, USA, Whitepaper*, pp. 1–47, 2020.
- [9] C. by Micron Technology Inc., “Ram memory speeds and compatibility,” 2023. [Online]. Available: <https://www.crucial.com/support/memory-speeds-compatibility>
- [10] M. Campanelli, D. Fiore, and A. Querol, “Legosnark: Modular design and composition of succinct zero-knowledge proofs,” in *Proceedings of the 2019 ACM SIGSAC Conference on Computer and Communications Security*, 2019, pp. 2075–2092.
- [11] B. Chen, B. Bünz, D. Boneh, and Z. Zhang, “HyperPlonk: Plonk with linear-time prover and high-degree custom gates,” *Cryptology ePrint Archive*, Paper 2022/1355, 2022. [Online]. Available: <https://eprint.iacr.org/2022/1355>
- [12] T. S. M. Company, “Tsmc 22nm technology,” 2021. [Online]. Available: https://www.tsmc.com/english/dedicatedFoundry/technology/logic/l_22nm
- [13] A. Daftardar, J. Mo, J. Ah-kiow, B. Bünz, R. Karri, S. Garg, and B. Reagen, “Need for zkspeed: Accelerating hyperplonk for zero-knowledge proofs,” *Cryptology ePrint Archive*, 2025.
- [14] A. Daftardar, B. Reagen, and S. Garg, “Szkp: A scalable accelerator architecture for zero-knowledge proofs,” in *Proceedings of the 2024 International Conference on Parallel Architectures and Compilation Techniques*, 2024, pp. 271–283.
- [15] N. Dhyani, J. C. Mo, P. Yubeaton, M. Cho, A. Joshi, S. Garg, B. Reagen, and C. Hegde, “Privit: Vision transformers for private inference,” *Transactions on Machine Learning Research*, 2024.
- [16] A. Ebel, K. Garimella, and B. Reagen, “Orion: A fully homomorphic encryption framework for deep learning,” in *Proceedings of the 30th ACM International Conference on Architectural Support for Programming Languages and Operating Systems, Volume 2*, 2025, pp. 734–749.
- [17] J. Erickson, *Algorithms*, 2023.
- [18] B. Feng, Z. Wang, Y. Wang, S. Yang, and Y. Ding, “Zeno: A type-based optimization framework for zero knowledge neural network inference,” in *Proceedings of the 29th ACM International Conference on Architectural Support for Programming Languages and Operating Systems, Volume 1*, ser. ASPLOS ’24. New York, NY, USA: Association for Computing Machinery, 2024, p. 450–464. [Online]. Available: <https://doi.org/10.1145/3617232.3624852>
- [19] A. Gabizon, Z. J. Williamson, and O. Ciobotaru, “PLONK: Permutations over lagrange-bases for oecumenical noninteractive arguments of knowledge,” *Cryptology ePrint Archive*, Paper 2019/953, 2019. [Online]. Available: <https://eprint.iacr.org/2019/953>
- [20] H. Geng, J. Mo, D. Reis, J. Takeshita, T. Jung, B. Reagen, M. Niemier, and X. S. Hu, “Privacy preserving in-memory computing engine,” *arXiv preprint arXiv:2308.02648*, 2023.
- [21] L. Grassi, D. Khovratovich, C. Rechberger, A. Roy, and M. Schofnegger, “Poseidon: A new hash function for zero-knowledge proof systems,” *Cryptology ePrint Archive*, Paper 2019/458, 2019. [Online]. Available: <https://eprint.iacr.org/2019/458>
- [22] S. Gully, V. Gopal, K. Yap, W. Feghali, J. Guilford, and G. Wolrich, “New instructions supporting the secure hash algorithm on intel architecture processors,” *Tech. Rep.*, 2013.
- [23] R. Inc., “White paper: Hbm2e and gddr6: Memory solutions for ai,” *White Paper*, Rambus Inc., 2020.
- [24] Intel, “Intel xeon gold 5218 processor (22m cache, 2.30 ghz) 2025,” 2025. [Online]. Available: <https://www.intel.com/content/www/us/en/products/sku/192444/intel-xeon-gold-5218-processor-22m-cache-2-30-ghz/specifications.html>
- [25] S. Kim, J. Kim, M. J. Kim, W. Jung, J. Kim, M. Rhu, and J. H. Ahn, “Bts: An accelerator for bootstrappable fully homomorphic encryption,” in *Proceedings of the 49th Annual International Symposium on Computer Architecture*, ser. ISCA ’22. New York, NY, USA: Association for Computing Machinery, 2022, p. 711–725. [Online]. Available: <https://doi.org/10.1145/3470496.3527415>
- [26] M. Knecht and C. U. Nicola, “A space- and time-efficient implementation of the merkle tree traversal algorithm,” *IMVS Fokus Report*, vol. 7, pp. 35–39, 2013. [Online]. Available: <http://hdl.handle.net/11654/17789;https://doi.org/10.26041/fhnw-562>
- [27] J. Mo, K. Garimella, N. Neda, A. Ebel, and B. Reagen, “Towards fast and scalable private inference,” in *Proceedings of the 20th ACM International Conference on Computing Frontiers*, 2023, pp. 322–328.
- [28] J. Mo, J. Gopinath, and B. Reagen, “Haac: A hardware-software co-design to accelerate garbled circuits,” in *Proceedings of the 50th Annual International Symposium on Computer Architecture*, ser. ISCA ’23. New York, NY, USA: Association for Computing Machinery, 2023. [Online]. Available: <https://doi.org/10.1145/3579371.3589045>
- [29] A. Nukada, “Performance optimization of allreduce operation for multi-gpu systems,” in *2021 IEEE International Conference on Big Data (Big Data)*. IEEE, 2021, pp. 3107–3112.
- [30] OpenCores, “Sha-3 ip core,” <https://opencores.org/projects/sha3>, 2013, accessed: November 16, 2024.
- [31] N. Samardzic, S. Langowski, S. Devadas, and D. Sanchez, “Accelerating zero-knowledge proofs through hardware-algorithm co-design,” Preprint, 2024, https://people.sail.mit.edu/devadas/pubs/micro24_nocap.pdf.
- [32] S. Schlachter and B. Drake, “Introducing micron® ddr5 sdram: More than a generational update,” *XP055844818*, vol. 31, p. 6, 2019.

- [33] S. Setty, "Spartan: Efficient and general-purpose zkSNARKs without trusted setup," in *Advances in Cryptology – CRYPTO 2020*, D. Micciancio and T. Ristenpart, Eds. Cham: Springer International Publishing, 2020, pp. 704–737.
- [34] S. Setty and J. Lee, "Quarks: Quadruple-efficient transparent zkSNARKs," *Cryptology ePrint Archive*, 2020.
- [35] R. M. Shadab, Y. Zou, S. Gandham, A. Awad, and M. Lin, "Hmt: A hardware-centric hybrid bonsai merkle tree algorithm for high-performance authentication," *ACM Transactions on Embedded Computing Systems*, vol. 22, no. 4, pp. 1–28, 2023.
- [36] J. Thaler, *Proofs, Arguments, and Zero-Knowledge*, 2022. [Online]. Available: <https://people.cs.georgetown.edu/jthaler/ProofsArgsAndZK.pdf>
- [37] R. S. Wahby, I. Tzialla, abhi shelat, J. Thaler, and M. Walfish, "Doubly-efficient zkSNARKs without trusted setup," *Cryptology ePrint Archive*, Paper 2017/1132, 2017. [Online]. Available: <https://eprint.iacr.org/2017/1132>
- [38] C. Wang and M. Gao, "Unizk: Accelerating zero-knowledge proof with unified hardware and flexible kernel mapping," in *Proceedings of the 30th ACM International Conference on Architectural Support for Programming Languages and Operating Systems, Volume 1*, ser. ASPLOS '25. New York, NY, USA: Association for Computing Machinery, 2025, p. 1101–1117. [Online]. Available: <https://doi.org/10.1145/3669940.3707228>
- [39] S.-Y. Wu, C. Y. Lin, M. Chiang, J. Liaw, J. Cheng, S. Yang, M. Liang, T. Miyashita, C. Tsai, B. Hsu *et al.*, "A 16nm finfet cmos technology for mobile soc and computing applications," in *2013 IEEE International Electron Devices Meeting*. IEEE, 2013, pp. 9–1.
- [40] S.-Y. Wu, C. Lin, M. Chiang, J. Liaw, J. Cheng, S. Yang, C. Tsai, P. Chen, T. Miyashita, C. Chang *et al.*, "A 7nm cmos platform technology featuring 4 th generation finfet transistors with a 0.027 um² high density 6-t sram cell for mobile soc applications," in *2016 IEEE International Electron Devices Meeting (IEDM)*. IEEE, 2016, pp. 2–6.
- [41] T. Xie, J. Zhang, Y. Zhang, C. Papamanthou, and D. Song, "Libra: Succinct zero-knowledge proofs with optimal prover computation," *Cryptology ePrint Archive*, Paper 2019/317, 2019. [Online]. Available: <https://eprint.iacr.org/2019/317>
- [42] T. Xie, Y. Zhang, and D. Song, "Orion: Zero knowledge proof with linear prover time," in *Advances in Cryptology - CRYPTO 2022 - 42nd Annual International Cryptology Conference, CRYPTO 2022, Santa Barbara, CA, USA, August 15-18, 2022, Proceedings, Part IV*, ser. Lecture Notes in Computer Science, Y. Dodis and T. Shrimpton, Eds., vol. 13510. Springer, 2022, pp. 299–328. [Online]. Available: https://doi.org/10.1007/978-3-031-15985-5_11
- [43] P. Yubeaton, J. C. Mo, K. Garimella, N. K. Jha, B. Reagen, C. Hegde, and S. Garg, "Truncformer: Private llm inference using only truncations," *arXiv preprint arXiv:2412.01042*, 2024.
- [44] N. Zhang, A. Ebel, N. Neda, P. Brinich, B. Reynwar, A. G. Schmidt, M. Franusich, J. Johnson, B. Reagen, and F. Franchetti, "Generating high-performance number theoretic transform implementations for vector architectures," in *2023 IEEE High Performance Extreme Computing Conference (HPEC)*. IEEE, 2023, pp. 1–7.
- [45] Z. Zhang, B. Chen, B. Bünz, and A. Xiong, "Hyperplonk implementation," 2022. [Online]. Available: <https://github.com/EsspressoSystems/hyperplonk>